

Self-dual Stacked Quantum Low-Density Parity-Check Codes

Ze-Chuan Liu^{1,*}, Chong-Yuan Xu^{1,*} and Yong Xu^{1,2†}

¹Center for Quantum Information, IIIS, Tsinghua University, Beijing 100084, People's Republic of China and
²Hefei National Laboratory, Hefei 230088, People's Republic of China

Quantum low-density parity-check (qLDPC) codes are promising candidates for fault-tolerant quantum computation due to their high encoding rates and distances. However, implementing logical operations using qLDPC codes presents significant challenges. Previous research has demonstrated that self-dual qLDPC codes facilitate the implementation of transversal Clifford gates. Here we introduce a method for constructing self-dual qLDPC codes by stacking non-self-dual qLDPC codes. Leveraging this methodology, we develop double-chain bicycle codes, double-layer bivariate bicycle (BB) codes, double-layer twisted BB codes, and double-layer reflection codes, many of which exhibit favorable code parameters. Additionally, we conduct numerical calculations to assess the performance of these codes as quantum memory under the circuit-level noise model, revealing that the logical failure rate can be significantly reduced with high pseudo-thresholds.

Given the inevitability of noise in quantum information processing, it is essential to utilize methods to mitigate its effects. Quantum error-correcting codes offer a feasible and reliable approach for achieving fault-tolerant quantum computation [1–9]. A prominent example is the surface code, which features local stabilizers and straightforward decoding procedures and has been experimentally demonstrated on quantum devices [10–14]. However, due to the low encoding rate of the surface code, implementing large-scale quantum computation incurs substantial resource overhead. Recently, qLDPC codes [6–9, 15–34], such as the BB code [9], have been introduced for fault-tolerant quantum computation. These codes provide a high encoding rate while maintaining a large code distance [9], making them promising candidates for low-overhead fault-tolerant quantum computation. In recent years, there has been growing interest in investigating their structure, performance, and potential extensions [35–39].

Despite the advantages of qLDPC codes, implementing logical gates remains a significant challenge. Existing methods, such as homomorphic measurements [40–42] and generalized lattice surgery [29, 43, 44], often require additional ancilla qubits and complex error correction procedures. Therefore, it is desirable to identify qLDPC codes that allow for transversal logical gate constructions. Recent studies indicate that self-dual qLDPC codes permit transversal Clifford gates [38, 45, 46]. Moreover, self-dual qLDPC codes can be utilized to construct fermionic codes for fermionic quantum computation based on Majorana modes [47–50]. While some self-dual qLDPC codes, such as bicycle codes [51] and certain BB codes [9, 38], exist, a general framework for constructing a self-dual code from a non-self-dual code remains undeveloped.

Here, we construct a class of self-dual Calderbank-Shor-Steane (CSS) LDPC codes by stacking non-self-dual CSS codes. We examine examples of double-chain bicycle codes, double-layer BB codes, double-layer twisted BB codes, and double-layer reflection codes. We calculate

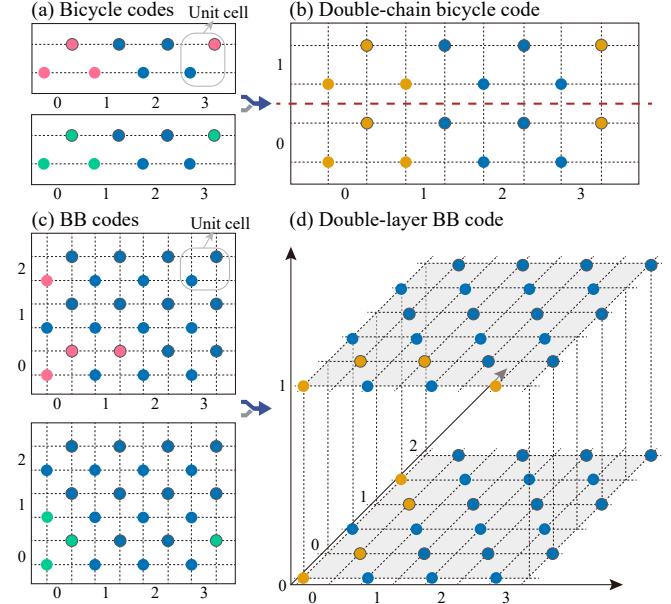


FIG. 1. Illustration of a double-chain bicycle code and a double-layer BB code obtained from a bicycle code with $A = I_4 + S_3^3$ and $B = I_4 + S_4$ and a BB code with $A = I_{12} + T_x$ and $B = I_{12} + T_y^2$, respectively. In (a) and (c), the support of an X (Z) stabilizer generator is highlighted by filled pink (green) circles in the upper (lower) panel. In (b) and (d), the support of an X (or Z) stabilizer generator is indicated by filled orange circles.

the parameters for each type of code and find that many exhibit odd-weight logical operators and exhibit favorable code parameters. Finally, we perform numerical simulations for several codes as qubit memory and observe that the logical failure rate can be significantly reduced, with the pseudo-threshold exceeding 0.7% under the circuit-level noise model.

Code construction.—We start by introducing our method to construct a self-dual CSS code based on a base CSS code that is not required to be self-dual. This base code is described by the X and Z stabilizer matrices, h_X

and h_Z , expressed as $h_X = (A \ B)$ and $h_Z = (B^T \ A^T)$, where A and B are square binary matrices. We require that $[A, B] = 0$, $[A, A^T] = 0$, and $[B, B^T] = 0$ so that $h_X h_Z^T = 0$, forming a well-defined code. We use the matrices A and B to construct new check matrices,

$$H_X = H_Z = \begin{pmatrix} A & B^T & A^T & B \\ B^T & A & B & A^T \end{pmatrix} = (U \ U^T), \quad (1)$$

where $U = I_2 \otimes A + \sigma_x \otimes B^T$ with I_l being an $l \times l$ identity matrix and σ_x being a Pauli matrix. It follows that $H_X H_Z^T = 0$ since $U U^T = U^T U$, thus obtaining a self-dual CSS code. If the base code is a qLDPC code, then the stacked code remains a qLDPC code, as the weight of stacked code's stabilizer generators is at most double maximum weight of the base code's stabilizer generators. We will use the bicycle code, BB code, and twisted BB code as base codes to construct self-dual codes. Finally, we propose a new class of base codes by introducing reflection operations to construct self-dual codes.

Double-chain bicycle code.—We first use the bicycle code [51] on a 1D periodic chain of length l to construct a double-chain bicycle code. In this setting, the matrices A and B are chosen to be circulant [51]. Specifically, A and B are expressed as $A = \sum_{j=0}^{l-1} a_j S_l^j$ and $B = \sum_{j=0}^{l-1} b_j S_l^j$, where $a_j, b_j \in \mathbb{Z}_2$ and S_l is the $l \times l$ cyclic shift matrix, whose only nonzero entry in row j appears in column $(j+1) \bmod l$. Clearly, A and B satisfy that $[A, B] = [A, A^T] = [B, B^T] = 0$, allowing the code to be used as a base code to construct self-dual double-chain bicycle codes. A base code's physical layout is obtained by placing each qubit at each lattice site for a lattice obtained by translating a unit cell consisting of two sites, as illustrated in Fig. 1(a). Given A and B , an X (Z) stabilizer generator for the base code called seed stabilizer is given by $s_X = \prod_j X_{0,j}^{a_j} \prod_{j'} X_{1,j'}^{b_{j'}}$ ($s_Z = \prod_j Z_{0,l-j}^{b_j} \prod_{j'} Z_{1,l-j'}^{a_{j'}}$), where $X_{\nu,j}$ ($Z_{\nu,j}$) denotes the Pauli X (Z) operator at the ν th site of the j th unit cell. All other generators are produced by translating this stabilizer while considering periodic boundary conditions (PBCs) [see Fig. 1(a) for an example]. For the self-dual code, two chains are included with the first and third block columns in the check matrix corresponding to the first chain and the second and fourth block columns corresponding to the second chain. The former and latter two block columns correspond to the upper and lower site in a unit cell, respectively. An X stabilizer generator is expressed as $S_X = \prod_{j_1} X_{0,(j_1,0)}^{a_{j_1}} \prod_{j_2} X_{0,(l-j_2,1)}^{b_{j_2}} \prod_{j_3} X_{1,(l-j_3,0)}^{a_{j_3}} \prod_{j_4} X_{1,(j_4,1)}^{b_{j_4}}$, where in (j, j_z) , j and j_z are the unit cell index and the chain index, respectively. An example is provided in Fig. 1(b).

Table I lists ten representative weight-eight double-chain bicycle codes (see more in Table V in End Matter) with parameters $[[n, k, d]]$ by considering $A = S_l^\alpha + S_l^\beta$

TABLE I. Weight-eight double-chain bicycle codes $[[n, k, d]]$ constructed from weight-four bicycle codes with $A = x^\alpha + x^\beta$ and $B = x^\gamma + x^\delta$, where $x = S_l$. Code distances are computed using the integer programming approach [9, 52]. The top five codes have logical operators of odd-weight, while the bottom five codes can only have logical operators of even-weight (the same holds for Table II–Table IV). Here, 1 represents an identity matrix.

$[[n, k, d]]$	l	A	B
$[[36, 4, 6]]$	9	$1 + x^4$	$x^3 + x^6$
$[[84, 12, 6]]$	21	$x^2 + x^5$	$x^5 + x^{14}$
$[[100, 12, 8]]$	25	$x^{10} + x^{24}$	$x^{10} + x^{16}$
$[[108, 4, 12]]$	27	$x^{22} + x^{24}$	$x^{12} + x^{22}$
$[[132, 8, 12]]$	33	$x^{10} + x^{11}$	$x^{11} + x^{31}$
$[[24, 8, 4]]$	6	$1 + x^2$	$x^3 + x^4$
$[[72, 6, 8]]$	18	$x^2 + x^{17}$	$x^4 + x^5$
$[[80, 8, 8]]$	20	$1 + x^{17}$	$x^8 + x^{17}$
$[[88, 4, 10]]$	22	$x^{13} + x^{18}$	$x + x^5$
$[[104, 6, 12]]$	26	$x^6 + x^{11}$	$x^5 + x^{14}$

and $B = S_l^\gamma + S_l^\delta$, where n , k , and d denote the number of physical qubits, the number of logical qubits, and code distance, respectively. These codes are obtained by numerically searching over various lattice sizes l and different parameters α , β , γ , and δ . The results indicate a high encoding rate. In addition, we observe that when l is even, it is highly probable that the code is an even code, meaning that the weight of logical operators cannot be odd. Conversely, when l is odd, the opposite holds true.

Double-layer BB code.—The BB code is a generalization of the bicycle code by considering $A = \sum_{j_x, j_y} a_{j_x j_y} T_x^{j_x} T_y^{j_y}$ and $B = \sum_{j_x, j_y} b_{j_x j_y} T_x^{j_x} T_y^{j_y}$, where $T_x = S_l \otimes I_m$ and $T_y = I_l \otimes S_m$ with l and m being positive integers, and $a_{j_x j_y}, b_{j_x j_y} \in \mathbb{Z}_2$ with j_x and j_y running from 0 to $l-1$ and $m-1$, respectively [9]. When $m=1$ or $l=1$, the code reduces to the bicycle code. The matrices A and B satisfy the required commutation relation for constructing the self-dual double-layer BB code. An analogous to the bicycle code, the physical arrangement of the BB codes corresponds to translating a unit cell comprising two qubits in the x and y directions, as illustrated in Fig. 1(c). For the matrices A and B presented above, the X (Z) seed stabilizer of the BB code is expressed as $s_X = \prod_{j_x, j_y} X_{0,(j_x, j_y)}^{a_{j_x j_y}} \prod_{j'_x, j'_y} X_{1,(j'_x, j'_y)}^{b_{j'_x j'_y}}$ ($s_Z = \prod_{j_x, j_y} Z_{0,(j_x, j_y)}^{a_{j_x j_y}} \prod_{j'_x, j'_y} Z_{1,(j'_x, j'_y)}^{b_{j'_x j'_y}}$), where the subscript $\nu, (j_x, j_y)$ denotes the qubit at the ν th site in a unit cell labeled by (j_x, j_y) . All other stabilizer generators can be obtained by translating this stabilizer along x and y . Similar to the double-chain bicycle code, the double-layer BB codes contain two layers with an X stabilizer generator (and similarly for Z stabilizer) written as $S_X = X_0 X_1 X_2 X_3$ with $X_0 = \prod_{j_{x1}, j_{y1}} X_{0,(j_{x1}, j_{y1}, 0)}^{a_{j_{x1} j_{y1}}}$, $X_1 =$

TABLE II. Weight-eight bilayer BB codes $[[n, k, d]]$ constructed from weight-four BB codes with $A = x^{\alpha_1}y^{\beta_1} + x^{\alpha_2}y^{\beta_2}$ and $B = x^{\gamma_1}y^{\delta_1} + x^{\gamma_2}y^{\delta_2}$, where $x = T_x$ and $y = T_y$.

$[[n, k, d]]$	l	m	A	B	kd^2/n
$[[60, 12, 5]]$	3	5	$x^2y^2 + x^2y$	$x^2y^2 + x^2$	5
$[[84, 8, 8]]$	3	7	$x^2y + x$	$x^2y^2 + x$	6.1
$[[100, 12, 8]]$	5	5	$xy + x^4y$	$y^2 + x^4y^3$	7.7
$[[108, 16, 6]]$	9	3	$x^2y^6 + x^3y^3$	$x^2y^4 + x^4y$	5.3
$[[140, 16, 8]]$	7	5	$y^4 + x^2y^2$	$y^2 + x^5y$	7.3
$[[56, 6, 8]]$	7	2	$y^4 + xy^3$	$x^5 + x^2y^3$	6.9
$[[80, 10, 8]]$	5	4	$y^2 + y$	$x^2y + x^4$	8
$[[112, 8, 12]]$	14	2	$x^3y^7 + x^{11}y^4$	$y^2 + x^5y^{12}$	10.3
$[[120, 8, 12]]$	6	5	$x^4 + x^5y^4$	$x + x^5y^3$	9.6
$[[160, 20, 8]]$	4	10	$y^3 + x^2y^2$	$x + x^3y^3$	8

$\prod_{j_{x2}, j_{y2}} X_{0, (j_{x2}, m - j_{y2}, 1)}^{b_{j_{x2}, j_{y2}}}$, $X_2 = \prod_{j_{x3}, j_{y3}} X_{1, (l - j_{x3}, j_{y3}, 0)}^{a_{j_{x3}, j_{y3}}}$, and $X_3 = \prod_{j_{x4}, j_{y4}} X_{1, (j_{x4}, j_{y4}, 1)}^{b_{j_{x4}, j_{y4}}}$, where the subscript includes a layer index. All other stabilizer generators are generated by translating this stabilizer while taking PBCs into account [see Fig. 1(a) for an example].

Table II presents weight-eight bilayer BB codes (see more in Table VI in End Matter) with parameters $[[n, k, d]]$ based on weight-four BB codes with $A = T_x^{\alpha_1}T_y^{\beta_1} + T_x^{\alpha_2}T_y^{\beta_2}$ and $B = T_x^{\gamma_1}T_y^{\delta_1} + T_x^{\gamma_2}T_y^{\delta_2}$ (see End Matter for more codes). We observe that when both l and m are even, the bilayer code is even, and when both are odd, it is highly probable that the code will be odd. Additionally, in cases where one is odd and the other is even, an even code typically achieves the maximum kd^2/n , although odd codes may also be found. Among these codes listed in the table, the maximum value of kd^2/n is 10.3 for the even-weight codes and 7.7 for the odd-weight codes.

Laurent polynomial formalism for the bilayer BB codes.—We now apply the theory of Laurent polynomials to describe the bilayer BB codes. Previously, this theory has been used to characterize the BB codes [35, 37]. Specifically, given two polynomial $f(x, y) = \sum_{j_x, j_y} a_{j_x j_y} x^{j_x} y^{j_y}$ and $g(x, y) = \sum_{j_x, j_y} b_{j_x j_y} x^{j_x} y^{j_y}$ in terms of two variables x and y , we represent a Pauli string using the vector $(f(x, y) \ g(x, y))$ whose support is defined by the exponents of the monomials in $f(x, y)$ and $g(x, y)$, corresponding to the seed stabilizer obtained for the code with $A = f(T_x, T_y)$ and $B = g(T_x, T_y)$ as discussed in previous sections. Thus, we use $(f(x, y) \ g(x, y))^T$ to represent the X seed stabilizer, from which all other X stabilizers can be derived by multiplying a polynomial from the Laurent polynomial ring $R_{xy} = \mathbb{Z}_2[x, y, x^{-1}, y^{-1}]$ to $(f(x, y) \ g(x, y))^T$. Similarly, the Z seed stabilizer is represented by $(\overline{g(x, y)} \ \overline{f(x, y)})^T$, where $\overline{(\dots)}$ denotes the antipode map, transforming all variables in the polynomial to their inverses, i.e., $x \mapsto$

TABLE III. Weight-eight double-layer twisted BB codes $[[n, k, d]]$ constructed from weight-four twisted BB codes with $A = x^{\alpha_1}y^{\beta_1} + x^{\alpha_2}y^{\beta_2}$ and $B = x^{\gamma_1}y^{\delta_1} + x^{\gamma_2}y^{\delta_2}$ with $x = T_x$ and $y = T_y$, where \tilde{T}_x with boundary twist γ is provided in End Matter.

$[[n, k, d]]$	l	m	γ	A	B	kd^2/n
$[[100, 12, 8]]$	5	5	3	$xy^3 + x^3y^3$	$x^2y^2 + x^4y^3$	7.7
$[[132, 8, 12]]$	3	11	9	$1 + x^2y^2$	$y^2 + x^1y$	8.7
$[[140, 16, 8]]$	5	7	1	$x^2y + y$	$x^2 + x^4y^2$	7.3
$[[180, 20, 8]]$	5	9	4	$y^3 + x$	$x^4y + xy^2$	7.1
$[[204, 8, 16]]$	17	3	2	$x^2y^5 + x^{14}y$	$x^{11}y^{16} + x^{13}y^{10}$	10
$[[112, 8, 12]]$	2	14	6	$y + xy$	$1 + y$	10.3
$[[128, 16, 8]]$	4	8	4	$xy + xy^3$	$x^2y^2 + xy^2$	8
$[[144, 8, 12]]$	2	18	10	$1 + y$	$y + xy$	8
$[[176, 10, 12]]$	11	4	1	$x^5y^2 + x^2y^8$	$x^{10}y + y^2$	8.2
$[[208, 8, 16]]$	26	2	1	$x^{10}y^{21} + x^7y^{21}$	$x^{10}y^4 + xy^{21}$	9.8

x^{-1} and $y \mapsto y^{-1}$. Within this formalism, the matrix T_x (T_y) can be viewed as a matrix representation of x of dimension l (y of dimension m) for R_{xy} . For example, when $f(x, y) = 1 + x^{-1}$ and $g(x, y) = 1 + y$, we obtain the toric code.

In our case, we introduce an additional variable z satisfying that $z^2 = 1$ and use the polynomial $u(x, y, z) = f(x, y) + zg(x, y)$ to describe the matrix U . The variable z thus serves to characterize the double layers. For instance, let $f(x, y) = 1 + x$ and $g(x, y) = 1 + y^2$. A seed X or Z stabilizer is then expressed as $(u(x, y, z) \ \overline{u(x, y, z)})^T = (1 + x + z(1 + y^{-2}) \ 1 + x^{-1} + z(1 + y^2))^T$ as shown in Fig. 1(d). All other X or Z stabilizers can be obtained by multiplying an element in the Laurent polynomial ring $R_{xyz} = \{f(x, y) + zg(x, y) : f(x, y), g(x, y) \in R_{xy}\}$ to $(u(x, y, z) \ \overline{u(x, y, z)})^T$.

We now follow Refs. [35–38, 53] to calculate the number of different types of excitations causing syndromes. Since our code is self-dual, it suffices to consider local Pauli Z strings that produce syndromes for X stabilizers. Let $S_X = (u_0(x, y, z) \ \overline{u_0(x, y, z)})^T$ with $u_0(x, y, z) \in R_{x,y,z}$ be an X seed stabilizer. We write a local Pauli Z string as $P = (f(x, y, z) \ g(x, y, z))^T$, where $f(x, y, z), g(x, y, z) \in R_{xyz}$. The syndromes generated by this Pauli string are given by $S_X \cdot P = u_0(x, y, z)f(x, y, z) + u_0(x, y, z)g(x, y, z)$, which indicates which X stabilizers anticommute with this Pauli string. For example, if $S_X \cdot P = 1 + x + xyz$, this indicates that the X stabilizer specified by $(0, 0, 0)$, $(1, 0, 0)$, and $(1, 1, 1)$ anticommutes with the string. The number of different types of excitations generated by Z Pauli strings is given by

$$k_{\max} = \dim(R_{xyz}/I_u), \quad (2)$$

where $I_u = \langle u, \overline{u} \rangle$ is an ideal generated by u and \overline{u} ,

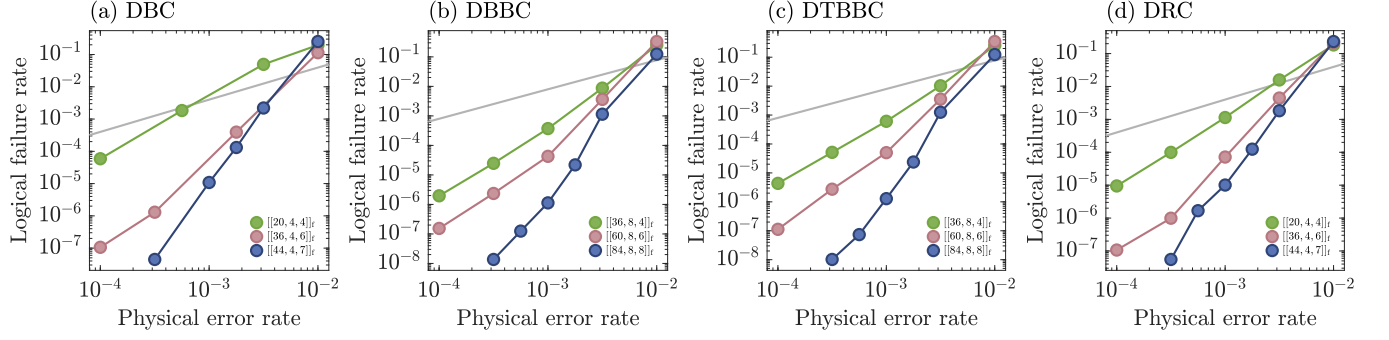


FIG. 2. Logical failure rate versus physical error rate under the circuit-level noise model for (a) double-chain bicycle codes (DBC), (b) double-layer BB codes (DBBC), (c) double-layer twisted BB codes (DTBBC), and (d) double-layer reflection codes (DRC). All of these codes have logical operators of odd-weight. The grey lines represent the probability of occurrence of an error on at least one physical qubit for k physical qubits, where k is the number of logical qubits in qubit memory.

TABLE IV. Weight-eight double-layer reflection codes $[[n, k, d]]$ constructed from weight-four reflection codes. Here, x, y, p , and q represent T_x, T_y, M_x , and M_y , respectively.

$[[n, k, d]]$	l	m	A	B	$\frac{kd^2}{n}$
$[[68, 4, 10]]$	17	1	$x^8y^5q + x^9y^{12}q$	$x^{11}y^2 + x^{15}y^{16}q$	5.9
$[[100, 12, 8]]$	5	5	$x^2py + x^2py^4$	$xy^2 + x^3y$	7.7
$[[120, 8, 10]]$	10	3	$x^2py^4 + xy^9$	$x^7y^4q + x^3y^7q$	6.7
$[[180, 20, 8]]$	15	3	$x^7y^8 + x^2y^{12}q$	$x^{14}y^{12}q + x^{10}y^{10}$	7.1
$[[252, 16, 16]]$	7	9	$x^6y^3q + x^5y$	$xy^3 + x^6y^6$	16.3
$[[64, 16, 8]]$	4	4	$xyq + xpy^3q$	$xyq + x^3py$	16
$[[96, 20, 8]]$	4	6	$x^3py^3 + xy$	$x^2y^2 + x^2y^3$	13.3
$[[120, 14, 10]]$	15	2	$x^{11}y^{14}q + x^7y^{14}$	$x^{10}y^6 + x^{11}y^{12}q$	11.7
$[[128, 32, 8]]$	8	4	$x^2py^6 + x^6$	$x^2y^5 + x^6yq$	16
$[[144, 16, 12]]$	18	2	$x^{11}y^6 + x^{15}y^{13}q$	$x^3q + x^{13}y^{10}$	16

$\dim(R_{xyz}/I_u)$ denotes the number of independent monomials in the quotient ring R_{xyz}/I_u , which can be calculated using the algorithm in Ref. [37]. Consequently, the number of logical qubits is $2k_{\max}$. For a specific lattice with width l and height m , PBCs impose the relations $x^l = 1$ and $y^m = 1$, modifying I_u to $\langle u, \bar{u}, x^l - 1, y^m - 1 \rangle$.

Double-layer twisted BB codes.—We now use twisted BB codes [37] as base codes to construct double-layer twisted BB codes. For a lattice of size $l \times m$, in contrast to the code with PBCs requiring that $x^l = 1$ and $y^m = 1$, a twisted code requires that $y^m = 1$ and $x^l y^{-\gamma} = 1$, where γ is an integer. This modification implies that, for a stabilizer, after translating it by l unit cells along x , a further translation of γ unit cells along y is required to return to the original stabilizer. See End Matter for the matrix form of x and y . The number of logical qubits in the double-layer twisted BB code can also be computed using the Laurent polynomial formalism described above in Eq. (2). The only modification lies in the set of algebraic relations imposed by the twisted boundary conditions, that is, $x^l y^{-\gamma} = 1$, modifying I_u to $\langle u, \bar{u}, x^l y^{-\gamma} - 1, y^m - 1 \rangle$. We provide ten representative

double-layer twisted BB codes in Table III and more in Table VII in End Matter.

Double-layer reflection code.—In the previous sections, we consider the A and B matrices, which are polynomials of either a cyclic shift matrix or commuting matrices T_x and T_y . Geometrically, all these matrices represent translation operations. We now introduce reflection operations M_x and M_y , which yield the mirror images of original sites with respect to the x -normal and y -normal planes, respectively. Their matrix representations are $M_x = M_l \otimes I_m$ and $M_y = I_l \otimes M_m$, where M_l is an $l \times l$ matrix whose entries are given by $[M_l]_{ij} = \delta_{i+j, l+1}$ for $1 \leq i, j \leq l$. Clearly, M_x and M_y do not commute with T_x and T_y . The check matrix A (and similarly B) is then modified to $A = \sum_{i,j,k,t} c_{i,j,k,t} T_x^i M_x^k T_y^j M_y^t$, where $c_{ijkt} \in \mathbb{Z}_2$. The constructed matrices A and B do not necessarily satisfy the conditions for base codes as described in the previous section. Therefore, we perform a numerical search to identify check matrices that satisfy the base code conditions, which are used to construct stacked codes. Ten codes are summarized in Table IV (see more in Table VIII in End Matter). Two of these codes can achieve a value of kd^2/n as large as 16 for similar-sized codes.

Numerical simulations.—We now perform a numerical examination of the noise resilience of the stacked qLDPC codes used as qubit memory under the circuit-level noise model. We first initialize all physical qubits in $|0\rangle$ and then consider the depolarizing noise with the physical error rate p . Subsequently, we perform $N_c = d$ rounds of syndrome extraction. The noise is modeled as the depolarizing noise channel occurring after each gate operation for both data qubits and ancilla qubits [54]. Additionally, we account for classical measurement readout errors in the ancilla qubits. At the end of the circuit, we perform a round of transversal measurement by measuring the Z operators of all physical data qubits. This transversal measurement yields the values of all Z stabilizers and the Z logical operators. We forward all

measurement results to a Tesseract decoder [55] to infer the values of all logical Z operators so as to determine whether a logical measurement value flip occurs. For N_{sample} samples, if N_{error} of them result in incorrect predictions from the decoder, then the logical error rate is $P_L(N_c) = N_{\text{error}}/N_{\text{sample}}$. The logical failure rate (LFR) is defined as $\text{LFR}(p) = 1 - (1 - P_L)^{1/N_c} \approx P_L/N_c$ [8, 9], which roughly indicates the logical error rate per syndrome cycle. The pseudo-threshold is defined as the error rate p_0 where $\text{LFR}(p_0) = 1 - (1 - p_0)^k$, meaning that the logical failure rate is equal to the probability that at least one error occurs for k physical qubits.

Figure 2 illustrates the logical failure rate as a function of the physical error rate for several stacked codes, including double-chain bicycle codes, double-layer BB codes, double-layer twisted BB codes, and double-layer reflection codes, all of which have logical operators of odd-weight (see End Matter for simulation results of stacked codes featuring even-weight logical operators). We see that the logical failure rate can be substantially suppressed, with the pseudo-threshold exceeding 0.7%.

In summary, we have introduced a general method for constructing self-dual qLDPC codes from non-self-dual qLDPC codes. The resulting codes can support logical operators of odd-weight while maintaining favorable parameters. Numerical simulations of several such codes as quantum memories further demonstrate that they can achieve a high pseudo-threshold.

We thank F. Wei, Y.-A. Chen, Y.-F. Mao, Y. Wu, and Z. Zhou for helpful discussions. This work is supported by the Innovation Program for Quantum Science and Technology (Grant No. 2021ZD0301604) and the National Natural Science Foundation of China (Grant No. 12474265 and No. 11974201). We also acknowledge the support by center of high performance computing, Tsinghua University.

2022 IEEE 63rd Annual Symposium on Foundations of Computer Science (FOCS) (IEEE, 2022) pp. 872–883.

- [8] Q. Xu, J. P. Bonilla Ataides, C. A. Pattison, N. Raveendran, D. Bluvstein, J. Wurtz, B. Vasić, M. D. Lukin, L. Jiang, and H. Zhou, Constant-overhead fault-tolerant quantum computation with reconfigurable atom arrays, *Nat. Phys.* **20**, 1084 (2024).
- [9] S. Bravyi, A. W. Cross, J. M. Gambetta, D. Maslov, P. Rall, and T. J. Yoder, High-threshold and low-overhead fault-tolerant quantum memory, *Nature* **627**, 778 (2024).
- [10] Y. Zhao, Y. Ye, H.-L. Huang, Y. Zhang, D. Wu, H. Guan, Q. Zhu, Z. Wei, T. He, S. Cao, *et al.*, Realization of an error-correcting surface code with superconducting qubits, *Phys. Rev. Lett.* **129**, 030501 (2022).
- [11] Suppressing quantum errors by scaling a surface code logical qubit, *Nature* **614**, 676 (2023).
- [12] D. Bluvstein, S. J. Evered, A. A. Geim, S. H. Li, H. Zhou, T. Manovitz, S. Ebadi, M. Cain, M. Kalinowski, D. Hangleiter, *et al.*, Logical quantum processor based on reconfigurable atom arrays, *Nature* **626**, 58 (2024).
- [13] Quantum error correction below the surface code threshold, *Nature* **638**, 920 (2025).
- [14] A. Eickbusch, M. McEwen, V. Sivak, A. Bourassa, J. Atalaya, J. Claes, D. Kafri, C. Gidney, C. W. Warren, J. Gross, *et al.*, Demonstration of dynamic surface codes, *Nat. Phys.* **1** (2025).
- [15] J.-P. Tillich and G. Zémor, Quantum ldpc codes with positive rate and minimum distance proportional to the square root of the blocklength, *IEEE Trans. Inf. Theory* **60**, 1193 (2013).
- [16] D. Gottesman, Fault-tolerant quantum computation with constant overhead, *Quantum Information and Computation* **14**, 1338 (2013).
- [17] A. A. Kovalev and L. P. Pryadko, Quantum kronecker sum-product low-density parity-check codes with finite rate, *Phys. Rev. A* **88**, 012311 (2013).
- [18] N. P. Breuckmann and B. M. Terhal, Constructions and noise threshold of hyperbolic surface codes, *IEEE Trans. Inf. Theory* **62**, 3731 (2016).
- [19] P. Panteleev and G. Kalachev, Degenerate quantum ldpc codes with good finite length performance, *Quantum* **5**, 585 (2021).
- [20] N. P. Breuckmann and J. N. Eberhardt, Balanced product quantum codes, *IEEE Trans. Inf. Theory* **67**, 6653 (2021).
- [21] A. Krishna and D. Poulin, Fault-tolerant gates on hypergraph product codes, *Phys. Rev. X* **11**, 011023 (2021).
- [22] O. Higgott and N. P. Breuckmann, Subsystem codes with high thresholds by gauge fixing and reduced qubit overhead, *Phys. Rev. X* **11**, 031039 (2021).
- [23] N. P. Breuckmann and J. N. Eberhardt, Quantum low-density parity-check codes, *PRX quantum* **2**, 040101 (2021).
- [24] P. Panteleev and G. Kalachev, Quantum ldpc codes with almost linear minimum distance, *IEEE Trans. Inf. Theory* **68**, 213 (2021).
- [25] N. Delfosse, M. E. Beverland, and M. A. Tremblay, Bounds on stabilizer measurement circuits and obstructions to local implementations of quantum ldpc codes, *arXiv:2109.14599* (2021).
- [26] N. Baspin and A. Krishna, Connectivity constrains quantum codes, *Quantum* **6**, 711 (2022).
- [27] N. Baspin and A. Krishna, Quantifying nonlocality: How

* These authors contribute equally to this work.

† yongxuphy@tsinghua.edu.cn

- [1] P. W. Shor, Scheme for reducing decoherence in quantum computer memory, *Phys. Rev. A* **52**, R2493 (1995).
- [2] A. Steane, Multiple-particle interference and quantum error correction, *Proc. Phys. Soc. A* **452**, 2551 (1996).
- [3] A. R. Calderbank and P. W. Shor, Good quantum error-correcting codes exist, *Phys. Rev. A* **54**, 1098 (1996).
- [4] R. Laflamme, C. Miquel, J. P. Paz, and W. H. Zurek, Perfect quantum error correction code, *Phys. Rev. Lett.* **77**, 198 (1996).
- [5] A. Y. Kitaev, Fault-tolerant quantum computation by anyons, *Ann. Phys.* **303**, 2 (2003).
- [6] P. Panteleev and G. Kalachev, Asymptotically good quantum and locally testable classical ldpc codes, in *Proceedings of the 54th annual ACM SIGACT symposium on theory of computing* (2022) pp. 375–388.
- [7] A. Leverrier and G. Zémor, Quantum tanner codes, in

outperforming local quantum codes is expensive, *Phys. Rev. Lett.* **129**, 050505 (2022).

[28] M. A. Tremblay, N. Delfosse, and M. E. Beverland, Constant-overhead quantum error correction with thin planar connectivity, *Phys. Rev. Lett.* **129**, 050504 (2022).

[29] L. Z. Cohen, I. H. Kim, S. D. Bartlett, and B. J. Brown, Low-overhead fault-tolerant quantum computing using long-range connectivity, *Sci. Adv.* **8**, eabn1717 (2022).

[30] A. Strikis and L. Berent, Quantum low-density parity-check codes for modular architectures, *PRX Quantum* **4**, 020321 (2023).

[31] A. O. Quintavalle, P. Webster, and M. Vasmer, Partitioning qubits in hypergraph product codes to implement logical gates, *Quantum* **7**, 1153 (2023).

[32] H.-K. Lin and L. P. Pryadko, Quantum two-block group algebra codes, *Phys. Rev. A* **109**, 022407 (2024).

[33] G. Zhang and Y. Li, Time-efficient logical operations on quantum low-density parity check codes, *Phys. Rev. Lett.* **134**, 070602 (2025).

[34] Y. Li, Low-density parity-check representation of fault-tolerant quantum circuits, *Phys. Rev. Res.* **7**, 013115 (2025).

[35] Z. Liang, Y. Xu, J. T. Iosue, and Y.-A. Chen, Extracting topological orders of generalized pauli stabilizer codes in two dimensions, *PRX Quantum* **5**, 030328 (2024).

[36] Z. Liang, B. Yang, J. T. Iosue, and Y.-A. Chen, Operator algebra and algorithmic construction of boundaries and defects in (2+ 1) d topological pauli stabilizer codes, [arXiv:2410.11942](https://arxiv.org/abs/2410.11942) (2024).

[37] Z. Liang, K. Liu, H. Song, and Y.-A. Chen, Generalized toric codes on twisted tori for quantum error correction, *PRX Quantum* **6**, 020357 (2025).

[38] Z. Liang and Y.-A. Chen, Self-dual bivariate bicycle codes with transversal clifford gates, [arXiv:2510.05211](https://arxiv.org/abs/2510.05211) (2025).

[39] K. Wang, Z. Lu, C. Zhang, G. Liu, J. Chen, Y. Wang, Y. Wu, S. Xu, X. Zhu, F. Jin, *et al.*, Demonstration of low-overhead quantum error correction codes, *Nat. Phys.*, 1 (2026).

[40] S. Huang, T. Jochym-O'Connor, and T. J. Yoder, Homomorphic logical measurements, *PRX Quantum* **4**, 030301 (2023).

[41] Q. Xu, H. Zhou, G. Zheng, D. Bluvstein, J. P. B. Ataides, M. D. Lukin, and L. Jiang, Fast and parallelizable logical computation with homological product codes, *Phys. Rev. X* **15**, 021065 (2025).

[42] B. Ide, M. G. Gowda, P. J. Nadkarni, and G. Dauphinain, Fault-tolerant logical measurements via homological measurement, *Phys. Rev. X* **15**, 021088 (2025).

[43] A. W. Cross, Z. He, P. J. Rall, and T. J. Yoder, Improved qldpc surgery: Logical measurements and bridging codes, [arXiv:2407.18393](https://arxiv.org/abs/2407.18393) (2024).

[44] A. Cowtan, Z. He, D. J. Williamson, and T. J. Yoder, Parallel logical measurements via quantum code surgery, [arXiv:2503.05003](https://arxiv.org/abs/2503.05003) (2025).

[45] T. Tansuwannont, Y. Takada, and K. Fujii, Clifford gates with logical transversality for self-dual css codes, [arXiv:2503.19790](https://arxiv.org/abs/2503.19790) (2025).

[46] K. Reddy and N. Kashyap, Asymptotically good css codes that realize the logical transversal clifford group fault-tolerantly, [arXiv:2601.08568](https://arxiv.org/abs/2601.08568) (2026).

[47] A. Schuckert, E. Crane, A. V. Gorshkov, M. Hafezi, and M. J. Gullans, Fermion-qubit fault-tolerant quantum computing, [arXiv:2411.08955](https://arxiv.org/abs/2411.08955) (2024).

[48] R. Ott, D. González-Cuadra, T. V. Zache, P. Zoller, A. M. Kaufman, and H. Pichler, Error-corrected fermionic quantum processors with neutral atoms, *Phys. Rev. Lett.* **135**, 090601 (2025).

[49] M. Mudassar, A. Schuckert, and D. Gottesman, Fault tolerant operations in majorana-based quantum codes: Gates, measurements and high rate constructions, [arXiv:2508.09928](https://arxiv.org/abs/2508.09928) (2025).

[50] C.-Y. Xu, Z.-C. Liu, and Y. Xu, Fermion-to-fermion low-density parity-check codes, [arXiv:2508.15323](https://arxiv.org/abs/2508.15323) (2025).

[51] D. J. C. MacKay, G. Mitchison, and P. L. McFadden, Sparse-graph codes for quantum error correction, *IEEE Trans. Inf. Theory* **50**, 2315 (2004).

[52] A. J. Landahl, J. T. Anderson, and P. R. Rice, Fault-tolerant quantum computing with color codes, [arXiv:1108.5738](https://arxiv.org/abs/1108.5738) (2011).

[53] J. N. Eberhardt and V. Steffan, Logical operators and fold-transversal gates of bivariate bicycle codes, *IEEE Transactions on Information Theory* (2024).

[54] C. Gidney, Stim: a fast stabilizer circuit simulator, *Quantum* **5**, 497 (2021).

[55] L. A. Beni, O. Higgott, and N. Shutty, Tesseract: A search-based decoder for quantum error correction, [arXiv:2503.10988](https://arxiv.org/abs/2503.10988) (2025).

End Matter

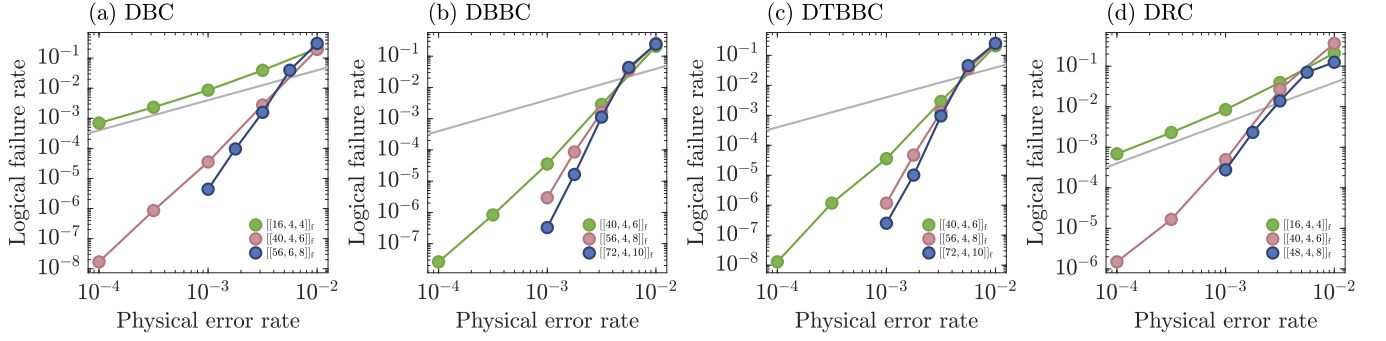


FIG. 3. Logical failure rate with respect to physical error rate under the circuit-level noise model for (a) double-chain bicycle codes, (b) double-layer BB codes, (c) double-layer twisted BB codes, and (d) double-layer reflection codes. All of these codes have logical operators of even-weight. The grey lines have the same meaning as those in Fig. 2. The error bars hidden behind filled circles represent the standard deviation of the logical failure rate, $\sigma_{LFR} = (1/N_c)(1 - P_L)^{\frac{1}{N_c}-1}\sigma_{P_L}$, where $\sigma_{P_L} = \sqrt{\frac{P_L(1-P_L)}{N_{\text{sample}}}}$ is the standard deviation of the logical error rate P_L [8, 9].

More details on the double-layer twisted BB codes.—For these codes, y corresponds to T_y and x corresponds to

$$\tilde{T}_x = \begin{pmatrix} 0 & I_m & 0 & 0 & \cdots & 0 \\ 0 & 0 & I_m & 0 & \cdots & 0 \\ \vdots & \vdots & \vdots & \vdots & \cdots & \vdots \\ 0 & 0 & 0 & 0 & \cdots & I_m \\ S_m^\gamma & 0 & 0 & 0 & \cdots & 0 \end{pmatrix}, \quad (3)$$

which is slightly different from T_x .

Simulation results of even stacked qLDPC codes.—Figure 3 presents the logical failure rate versus the physical failure rate for the four types of stacked codes with even-weight logical operators. We see that the pseudo-threshold can reach up to 0.5%.

TABLE V. More weight-eight double-chain bicycle codes, continuation of Table I.

$[[n, k, d]]$	l	A	B	$\frac{kd^2}{n}$	Type	$[[n, k, d]]$	l	A	B	$\frac{kd^2}{n}$	Type
$[[116, 4, 14]]$	29	$1 + x^3$	$x^{20} + x^{25}$	6.8	odd	$[[240, 28, \leq 6]]$	60	$x^{41} + x^{59}$	$x^4 + x^{26}$	4.2	even
$[[132, 8, 12]]$	33	$x^{10} + x^{11}$	$x^{11} + x^{31}$	8.7	odd	$[[248, 4, \leq 20]]$	62	$x^7 + x^{26}$	$x^{32} + x^{34}$	6.5	even
$[[148, 4, 16]]$	37	$x^{21} + x^{24}$	$x^{17} + x^{22}$	6.9	odd	$[[264, 8, \leq 16]]$	66	$x^4 + x^{18}$	$x^{42} + x^{53}$	7.8	even
$[[176, 16, 8]]$	44	$x^{11} + x^{31}$	$1 + x^8$	5.8	odd	$[[280, 4, \leq 22]]$	70	$x^{25} + x^{51}$	$x^{21} + x^{64}$	6.9	even
$[[204, 4, \leq 18]]$	51	$1 + x^{14}$	$x^{32} + x^{40}$	6.4	odd	$[[296, 6, \leq 18]]$	74	$x^6 + x^{65}$	$x^8 + x^{25}$	6.6	even
$[[276, 12, \leq 12]]$	69	$x^{27} + x^{33}$	$x^{15} + x^{54}$	6.3	odd	$[[312, 6, \leq 20]]$	78	$x^{14} + x^{73}$	$x^2 + x^{71}$	7.7	even
$[[380, 12, \leq 16]]$	95	$x^2 + x^{25}$	$x^{58} + x^{75}$	8.1	odd	$[[360, 4, \leq 24]]$	90	$x^{22} + x^{24}$	$x + x^{52}$	6.4	even

TABLE VI. More weight-eight double-layer BB codes, continuation of Table II. The codes on the right-hand side have even-weight logical operators.

$[[n, k, d]]$	l	m	A	B	$\frac{kd^2}{n}$	Type	$[[n, k, d]]$	l	m	A	B	$\frac{kd^2}{n}$
$[[60, 12, 5]]$	3	5	$x^2y^2 + x^2y$	$x^2y^2 + x^2$	5	odd	$[[104, 6, 12]]$	13	2	$x^2y^8 + x^9y$	$x^7y + x^6y^8$	8.3
$[[156, 12, 10]]$	13	3	$y^6 + x^{10}y^{12}$	$x^{10}y^{11} + x^8y^8$	7.7	odd	$[[128, 16, 8]]$	16	2	$x^7y^9 + x^8y^9$	$x^5y^9 + x^2y^{11}$	8
$[[204, 8, \leq 16]]$	17	3	$x + x^6y^{10}$	$x^2y^{12} + x^6y^{11}$	10	odd	$[[168, 6, 16]]$	6	7	$y^4 + x^3y$	$y^5 + x^5$	9.1
$[[228, 4, \leq 20]]$	19	3	$x^{17}y^{13} + x^{11}y^{13}$	$x^{13} + x^{18}y$	7	odd	$[[192, 24, 8]]$	12	4	$x^2y^3 + x^7y^9$	$x^2y^{10} + x^{11}y^2$	8
$[[260, 20, \leq 10]]$	5	13	$x^4y^2 + x^{41}$	$x^2 + x^2y^3$	7.7	odd	$[[208, 12, \leq 12]]$	26	2	$x^{21}y^9 + x^{24}y^{17}$	$x^{20}y^4 + xy^4$	8.3
$[[276, 4, \leq 22]]$	23	3	$x^{20}y^{19} + x^{16}y^{12}$	$x^{17}y^{18} + x^8y^9$	7	odd	$[[216, 16, \leq 10]]$	6	9	$x^2 + x^2y^5$	$y^3 + x^3y^2$	7.4
$[[280, 32, \leq 8]]$	7	10	$xy^5 + x^4y^3$	$x^3y^3 + x^6y^3$	7.3	odd	$[[224, 16, \leq 12]]$	4	14	$x^3y^3 + xy$	$x^3y + x^{11}$	10.3
$[[364, 28, \leq 10]]$	7	13	$y^5 + y^4$	$xy + xy^6$	7.7	odd	$[[248, 6, \leq 20]]$	31	2	$x^{29}y^{25} + x^3y^{22}$	$x^{29}y^{28} + x^{22}y^{11}$	9.7
$[[24, 8, 4]]$	3	2	$xy^2 + x^2$	$x^2y + xy^2$	5.3	even	$[[272, 8, \leq 20]]$	17	4	$x^9y^{11} + x^{10}y^8$	$x^{31} + xy^{11}$	11.8
$[[32, 12, 4]]$	2	4	$xy + x$	$x + y$	6	even	$[[288, 12, \leq 16]]$	9	8	$x^7y^8 + x^4y^3$	$x^8y^2 + x^7y^7$	10.7
$[[64, 24, 4]]$	4	4	$x^3y^3 + x$	$xy^2 + xy^3$	6	even	$[[320, 16, \leq 16]]$	10	8	$x^7y^8 + x^9y^9$	$x^5y^6 + y$	12.8
$[[88, 4, 12]]$	11	2	$y^7 + xy$	$x^9y^4 + x^7y^7$	6.5	even	$[[384, 48, \leq 8]]$	12	8	$xy^4 + xy^{10}$	$x^5y^{11} + x^8y^8$	8

TABLE VII. More weight-eight double-layer twisted BB codes, continuation of Table III. The codes on the right-hand side have even-weight logical operators.

$[[n, k, d]]$	l	m	γ	A	B	$\frac{kd^2}{n}$	Type	$[[n, k, d]]$	l	m	γ	A	B	$\frac{kd^2}{n}$
$[[60, 12, 5]]$	3	5	4	$x^2 + x^2y$	$1 + y^2$	5	odd	$[[56, 6, 8]]$	7	2	1	$xy^5 + x^6y^3$	$x^4y^4 + x^5y^4$	6.9
$[[84, 8, 8]]$	3	7	4	$1 + xy^2$	$y^2 + x^2y^2$	6.1	odd	$[[64, 8, 8]]$	2	8	5	$y + x$	$xy + 1$	8
$[[100, 12, 8]]$	5	5	3	$xy^3 + x^3y^3$	$x^2y^2 + x^4y^3$	7.7	odd	$[[72, 4, 10]]$	3	6	2	$xy + x^2$	$y^2 + x^2y^2$	5.6
$[[220, 12, \leq 12]]$	11	5	2	$x^9y^9 + x^2y^2$	$x^7 + x^9y^5$	7.9	odd	$[[80, 10, 8]]$	10	2	1	$x^9y^3 + y^8$	$x^5 + x^2y^9$	8
$[[228, 8, \leq 16]]$	3	19	1	$y^2 + x$	$1 + x^2y^2$	9.0	odd	$[[104, 6, 12]]$	2	13	6	$xy + 1$	$x + y$	8.3
$[[252, 4, \leq 20]]$	7	9	4	$x^2y^4 + x^2$	$x^3y + x^6y^4$	6.3	odd	$[[120, 8, 12]]$	3	10	7	$x^2 + x$	$x^2y + xy^2$	9.6
$[[260, 4, \leq 21]]$	5	13	10	$x^4y + x^2y^4$	$x^4 + 1$	6.8	odd	$[[136, 6, 12]]$	2	17	12	$x + y$	$x + 1$	6.4
$[[324, 8, \leq 20]]$	3	27	9	$x^2y + y^2$	$xy^2 + x^2y^2$	9.9	odd	$[[160, 20, 8]]$	4	10	1	$x^2y + y^2$	$x^2y^2 + 1$	8
$[[340, 4, \leq 22]]$	5	17	14	$y^4 + y^3$	$x^4 + x^3y$	5.7	odd	$[[216, 12, \leq 12]]$	6	9	3	$x^5y^3 + x^5y^4$	$y^3 + x^5y^2$	8
$[[372, 8, \leq 18]]$	3	31	16	$xy^2 + y^2$	$x^2y^2 + y$	7.0	odd	$[[224, 16, \leq 12]]$	4	14	2	$x^3y^2 + xy$	$x^3y^3 + x^3$	10.3
$[[24, 8, 4]]$	3	2	1	$y^2 + x^2y$	$y + x$	5.3	even	$[[240, 16, \leq 12]]$	6	10	2	$y^3 + x^5y$	$x^4y^2 + y^5$	9.6
$[[32, 12, 4]]$	2	4	1	$xy + 1$	$x + 1$	6	even	$[[288, 12, \leq 16]]$	8	9	1	$x^5y^4 + y^3$	$x^5y^2 + x^2y^5$	10.7
$[[48, 16, 4]]$	2	6	2	$y + xy$	$xy + x$	5.3	even	$[[384, 8, \leq 20]]$	3	32	6	$y + xy^2$	$x^2y + xy^2$	8.3

TABLE VIII. More weight-eight double-layer reflection codes, continuation of Table IV. The codes on the left-hand and right-hand sides have odd-weight and even-weight logical operators, respectively.

$[[n, k, d]]$	l	m	A	B	$\frac{kd^2}{n}$		$[[n, k, d]]$	l	m	A	B	$\frac{kd^2}{n}$
$[[28, 4, 5]]$	7	1	$x^2y^2 + x^5y^6q$	$x^3y^3q + xy^6q$	3.6		$[[24, 8, 4]]$	3	2	$y^2q + xyq$	$x^2y + q$	5.3
$[[36, 12, 4]]$	3	3	$pyq + x$	$pq + xy^2q$	5.3		$[[32, 18, 4]]$	4	2	$x^3y^3 + xpy^3q$	$x^3py^3 + x^3$	9
$[[44, 4, 7]]$	11	1	$x^9y^8 + x^2y^3q$	$xy^2 + x^7y^2$	4.5		$[[96, 20, 8]]$	4	6	$x^3py^3 + xy$	$x^2y^2 + x^2y^3$	13.3
$[[60, 12, 5]]$	15	1	$y^2 + x^6y^{10}$	$x^{10}y^9q + x^7y^7$	5		$[[112, 8, 14]]$	14	2	$x^5y^3 + x^6q$	$x^{10}y^{12}q + x^5y^5q$	14
$[[132, 4, 18]]$	11	3	$x^7y^2 + x^6$	$x^{10}y^{10}q + x^7yq$	9.8		$[[120, 14, 10]]$	15	2	$x^{11}y^{14}q + x^7y^{14}$	$x^{10}y^6 + x^{11}y^{12}q$	11.7
$[[260, 4, \leq 26]]$	13	5	$x^{12}y^7 + x^7y^3$	$x^{10}y^2q + x^{11}y^9q$	10.4		$[[160, 8, 16]]$	10	4	$x^2y^8 + x^6y$	$x^7y^3q + y^5q$	12.8
$[[300, 4, \leq 28]]$	25	3	$x^3y^5 + x^{24}y^4$	$x^{14}y^6 + x^{19}y^2q$	10.5		$[[200, 4, \leq 20]]$	25	2	$x^{15}y^2q + x^2y^{15}q$	$x^4y^{22}q + x^{13}y^4q$	8
$[[324, 4, \leq 28]]$	27	3	$x^2y^4 + x^6y^{17}$	$x^{22}y^{17}q + x^{16}y^{14}q$	9.7		$[[256, 8, \leq 20]]$	32	2	$x^{28}y^6 + x^9y^{22}q$	$x^{13}y^{26}q + x^{15}y^6q$	12.5
$[[348, 4, \leq 35]]$	29	3	$x^{21}y^5 + x^{24}y^{10}q$	$x^{27}y^{19}q + x^{22}y^{20}$	14.1		$[[312, 6, \leq 30]]$	13	6	$x^{11}y^7q + y^5$	$xy^5 + x^5y^7q$	17.3
$[[380, 4, \leq 58]]$	5	19	$x^4y^3 + x^3py^4$	$xy + x^4y^3$	35.4		$[[384, 24, \leq 16]]$	24	4	$x^{16}y^8 + x^5y^2$	$x^{13}y^{11}q + x^{10}y^{11}$	16